Phonon Dispersion and Proton Disorder of Ice VII and VIII

G. Radtke,[1,*] S. Klotz,[1,†] M. Lazzeri,[1] P. Loubeyre,[2] M. Krisch,[3] and A. Bossak[3]
[1]Sorbonne Université, CNRS UMR 7590, MNHN, IRD, Institut de Minéralogie, de Physique des Matériaux et de Cosmochimie (IMPMC), 4 place Jussieu, CEDEX 05, 75252 Paris, France
[2]CEA, DAM, DIF, 91297 Arpajon Cedex, France and Université Paris-Saclay, CEA, Laboratoire Matière en Conditions Extrêmes, 91680 Bruyères le Châtel, France
[3]European Synchrotron Radiation Facility (ESRF), 71 Avenue des Martyrs, 38000 Grenoble, France

(Received 21 March 2023; revised 29 September 2023; accepted 16 November 2023; published 31 January 2024)

The phonon dispersion of ice VII and that of its proton-ordered analog ice VIII are investigated through a combination of inelastic x-ray scattering (IXS) measurements and first-principles calculations of the oxygen sublattice dynamic structure factor. Particular attention is devoted to hydrogen-disorder in ice VII, addressed theoretically through a statistical ensemble of fictitious ordered supercell configurations. Similar phonon densities of states are found in both phases but are significantly less structured in the case of ice VII. Our data further show that, despite a full proton disorder, the acoustic phonon branches in this phase clearly inherit the periodicity of its body-centered cubic oxygen lattice. The calculations predict, however, the presence of gap openings in the one-atom phonon dispersion. These predictions are supported by revisiting the analysis of previous single-crystal IXS measurements along the longitudinal [111] branch of ice VII.

DOI: 10.1103/PhysRevLett.132.056102

Ice VII and VIII are the dominant high pressure phases of solid water [1]. Among the ∼20 ice phases known presently [2], the two forms are remarkable in several aspects: their extreme stability under compression over more than 50 GPa, their relatively simple structures, and the fact that ice VII is the fully hydrogen-disordered form of ice VIII. Specifically, ice VII crystallizes above 2 GPa in space group $Pn\bar{3}m$ with only two molecules per unit cell and oxygen at a body-centered cubic (bcc) lattice (Fig. 1). It is hence considered the simplest ice structure known. Upon cooling to below ≈270 K (at 2 GPa) it converts to its fully hydrogen-ordered form ice VIII which is tetragonal ($I4_1/amd$) with eight molecules per unit cell. Ice VII was recently found in diamond inclusions and is hence a mineral [3]. Given the fundamental role of water and ice, the dynamical properties of various forms of solid water appear to be of major academic and practical interest. However, there is very little experimental data on the full phonon dispersion of ice phases. In fact, complete phonon dispersion curves have been measured only for a single ice phase, i.e. ordinary ice I_h [4,5]. For all other ice phases, and specifically here for ice VIII, information on the lattice dynamics relies on optical (Raman, infrared) data and incoherent neutron scattering [6–10], all obtained on powder samples with their well-known limitations.

Here, we use inelastic x-ray scattering (IXS) on macroscopic *powder* samples of ice VII and VIII recovered to ambient pressure, coupled to first-principles calculations to determine the phonon dispersion of both phases. For ice VII, the results will further be compared to data obtained by reinvestigating IXS *single-crystal* measurements in a diamond anvil cell [11]. Compared to previous inelastic incoherent neutron measurements [6,7], IXS allows one to collect data at various defined momentum transfers and to determine the phonon density of states of oxygen only, hence avoiding the complicated contributions of hydrogen with its site disorder in the case of ice VII. A series of questions then arise which will be addressed in this Letter: How does proton disorder affect the acoustic branches of ice VII? To which extent is it possible to consider its dynamics as that of an actual bcc crystal? Are the concepts of transverse and longitudinal acoustic phonons still meaningful in such a case?

For the powder measurements, approximately 80 mm^3 of ice VIII was obtained by compression of liquid water to 4 GPa, cooling to 80 K and decompression to 0 GPa, all done in a Paris-Edinburgh press [12]. The synthesis of ice VII used the same technique, but a different pressure-temperature path, i.e. compression of ice VI at low temperatures to 5–7 GPa. It was shown previously [13] that this method gives pure, metastable ice VII which then can be decompressed and extracted from the pressure cell similar to ice VIII. The inelastic x-ray scattering measurements were carried out at the ID28 beamline of the ESRF (Grenoble, France) with 0.5701 Å radiation and an energy resolution of 1.7 meV using the (11,11,11) reflection of a set of 5 silicon analyzers. The sample pellets were ground under liquid nitrogen to obtain a perfect powder sample and transferred at 77 K to a closed-cycle refrigerator which kept the temperature at 30 K during the entire experiment. ID28

allows one to collect diffraction pattern (zero energy transfer) which confirmed pure ice VII and ice VIII phases.

Figure 1 shows two examples of constant-$|\mathbf{Q}|$ scans for ice VIII in (b) and (c) and for ice VII in (e) and (f) at different modules of the scattering vector (see Supplemental Material (SM) [14] for additional data). The observed maxima occur at $|\mathbf{Q}|$ values where the specific scan crosses certain branches of the phonon dispersion. All the structures visible in Fig. 1, extending up to about 35 meV, are primarily associated to phonons involving the rigid translation of water molecules. Librational modes starting at 55 meV [15] as well as modes involving molecular internal degrees of freedom at higher energies, are too weak to be detected in such measurements due to the very small scattering power of hydrogen. For a given $|\mathbf{Q}|$ value, the ice VII and VIII energy scans are generally similar, as expected from their closely related structures. However, the spectra of H-ordered ice VIII are significantly more structured than those of the fully H-disordered counterpart ice VII. The minimum at 25 meV in the $|\mathbf{Q}| = 59.2$ nm^{-1} spectrum in ice VIII is, for instance, completely wiped out in ice VII.

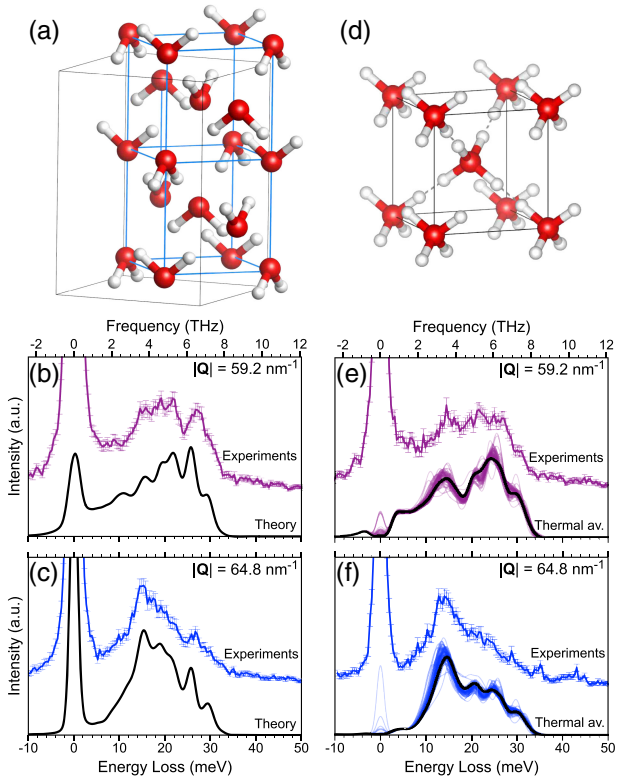

FIG. 1. Structure of tetragonal ice VIII in (a) and cubic ice VII in (d) with oxygen drawn in red and hydrogen sites in white. In ice VII, the four possible hydrogen sites around an oxygen atom are occupied only 50% averaged over space and time. On the contrary, in ice VIII the H-site is 100% occupied. In (a), the unit cell of ice VIII is drawn in black and the associated unit cell of ice VII in blue. Examples of constant-$|\mathbf{Q}|$ scans (colored lines with error bars) of ice VIII in (b),(c) and ice VII in (e),(f) collected at 30 K and ambient pressure. Experiments are compared to first-principles calculations (thick black lines). For ice VII, the average spectrum is superimposed to the 52 supercell contributions (thin colored lines). A Gaussian broadening of full width at half maximum of 1.7 meV was employed to account for the instrumental energy resolution.

These spectra have been modeled using density functional theory calculations as implemented in the QUANTUM ESPRESSO suite of codes [16]. Optimized norm-conserving pseudopotentials [17] were employed with a plane-wave cutoff energy of 80 Ry and the Perdue-Burke-Ernzerhof (PBE) functional [18], which has already been shown to provide a good description of different phases of ice [19–21]. Total energies were obtained using the lattice parameters of ice VII and VIII measured at 77 K prior to the IXS experiments and optimizing atomic positions only. Phonons were then calculated from linear response [22].

The IXS dynamic structure factor (DSF) [23] for one-phonon scattering was calculated entirely from first principles within the spherical rigid-ion approximation. This approximation is particularly well justified here as we are only considering large scattering vectors and thus mainly probing electron density at the ionic cores [24]. We further assumed a purely ionic picture of water molecules built from H^+ and O^{2-} ions and, therefore, considered the latter as the only x-ray scatterers. The polycristallinity of the samples was taken into account by integrating this partial oxygen-oxygen DSF over a sphere of radius $|\mathbf{Q}|$ in the reciprocal space. In the case of ice VII, the hydrogen disorder was accounted for by considering the 52 symmetrically distinct, ice-rule-allowed configurations compatible with a $2 \times 2 \times 2$ cubic supercell containing 16 water molecules [25–27] (see SM [14]). The partial DSF of the resulting ensemble of fictitious ordered configurations weighted by their statistical probability was then employed to calculate configurational average spectra mimicking the physical disorder characterizing ice VII

$$\langle S^{\mathrm{IXS}}_{1\mathrm{ph}}(|\mathbf{Q}|,\omega)_{\mathrm{OO}}\rangle = \sum_{c=1}^{52} \frac{g_c e^{-\beta E_c}}{\mathcal{Z}} S^{\mathrm{IXS}}_{1\mathrm{ph}}(|\mathbf{Q}|,\omega)^c_{\mathrm{OO}}. \quad (1)$$

In this expression, g_c and E_c are, respectively, the degeneracy and the total energy of configuration c, $\beta = 1/k_{\mathrm{B}}T$, and $\mathcal{Z}$ is the configurational partition function. A temperature $T = 293$ K was chosen here since the diffraction pattern (hence the structure) of recovered ice VII is indistinguishable from those collected at ambient temperature, apart from the change of lattice parameter and the temperature-dependent Debye-Waller factor [13]. The results are shown as black lines in Fig. 1. In the case of ice VII, the individual contributions corresponding to the 52 supercell configurations are also shown to give an insight into the sensitivity of the spectral features to the variations of H-bond ordering. The comparison with experimental findings shows a remarkable agreement. Theory correctly predicts all characteristic features displayed by the experimental spectra, and for all measured $|\mathbf{Q}|$ values (see also SM [14]).

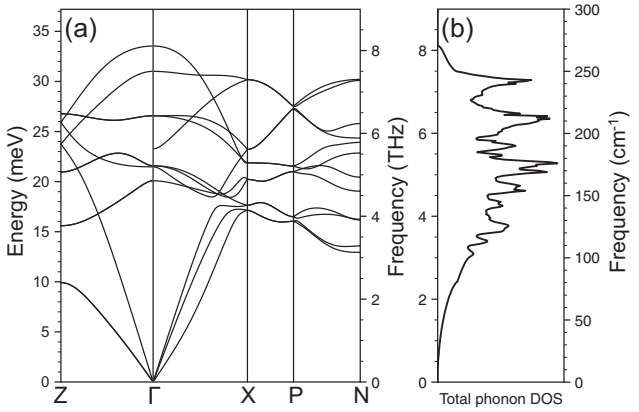

FIG. 2. Phonon dispersion of ice VIII in (a) and phonon density of states in (b) obtained by first-principles calculations.

Figure 2 presents the corresponding theoretical low-frequency phonon dispersion of ice VIII. With 4 water molecules per primitive unit cell, the phonon spectrum reveals 12 branches involving predominantly the rigid translation of water molecules. Libration modes arising at higher energies as well as modes involving internal degrees of freedom of the molecules are not presented here. Dispersions are in fair agreement with those published previously [28,29]. For zone-center frequencies in the relevant energy range, our calculations predict Raman modes to be observed at 173.2 cm^{-1} (A_{1g}), 174.1 cm^{-1} (E_g), 214.3 cm^{-1} (E_g), and 270.5 cm^{-1} (B_{1g}). This compares very favorably with the experimental Raman bands reported by Wong and Whalley [8] at 169.2 cm^{-1}, 172.0 cm^{-1}, 214.3 cm^{-1}, and 258.2 cm^{-1} at 0 GPa and 100 K.

The accuracy of our approach being assessed, we can now address the considerably more challenging case of ice VII by analyzing the calculated vibrational modes through

$$S^{\mathrm{OO}}_{\hat{\mathbf{n}}}(\mathbf{Q},\omega) = \frac{\hbar}{2MN}\sum_j \frac{1}{\hbar\omega_j(\mathbf{q})}\left|\sum_{\kappa\in \mathrm{Oxy.}} \hat{\mathbf{n}}\cdot\mathbf{e}(\kappa|\mathbf{q}j)e^{-i\mathbf{Q}\cdot\mathbf{r}(\kappa)}\right|^2 \delta[\hbar\omega-\hbar\omega_j(\mathbf{q})], \tag{2}$$

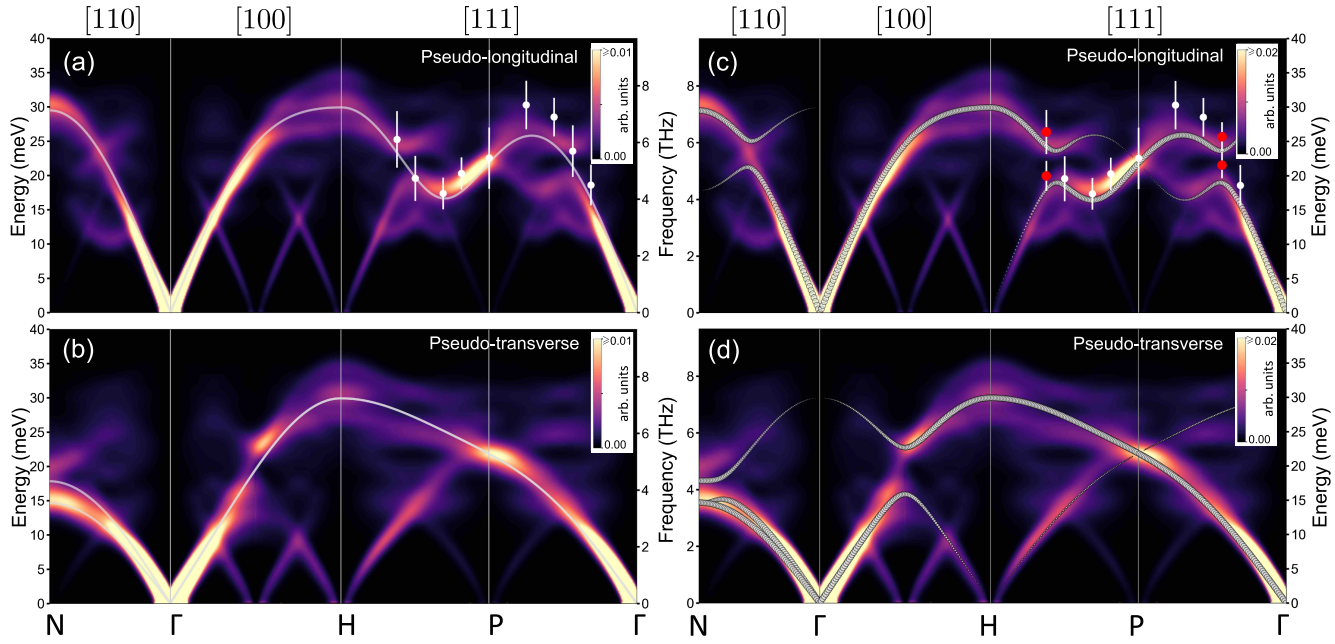

FIG. 3. Phonon dispersion of ice VII. The color-coded intensity map corresponds to ensemble-averaged $\langle S^{\mathrm{OO}}_{\hat{\mathbf{n}}}(\mathbf{Q},\omega)\rangle$ along high symmetry directions of the extended Brillouin zone of the oxygen body-centered cubic sublattice. The unit vector $\hat{\mathbf{n}}$ was chosen to be either parallel to $\hat{\mathbf{Q}}$ to reveal the longitudinal character of phonon modes in (a) and (c) or perpendicular to $\hat{\mathbf{Q}}$ to reveal the transverse character of the modes in (b) and (d). The dispersion obtained when describing ice VII as a monoatomic bcc crystal using a very simple Born-von Kármán model is superimposed (white lines) in (a) and (b). The phonon dispersion of a refined model describing ice VII as two interpenetrating diamond sublattices unfolded in the extended Brillouin zone of the bcc oxygen sublattice (gray circles) is shown in (c) and (d). Energies and full width at half-maximum extracted from fitting the spectra acquired on a single crystal with a single pseudo-Voigt (white dots) are shown in (a) and using two pseudo-Voigt functions (red dots) for $|\mathbf{Q}| = 7$ and 26 nm^{-1} in (c).

where M, N, and $\mathbf{r}(\kappa)$ are, respectively, the mass, total number, and position of the oxygen ions in one supercell, $\mathbf{Q} = \mathbf{q} + \mathbf{G}$ where $\mathbf{q}$ is the phonon wavevector in the first Brillouin zone and $\mathbf{G}$ is a reciprocal-lattice vector. j and κ are branch and atomic indexes, κ running only on the oxygen, $\mathbf{e}(\kappa|\mathbf{q}j)$ is the polarization vector, normalized in the supercell, of the phonon of energy $\hbar\omega_j(\mathbf{q})$. S^{OO} is strictly related to the oxygen-oxygen correlation function (see SM [14]) and provides a natural way to unfold the vibrations of a supercell (containing 16 water molecules) into vibrations of the simple bcc cell, excluding hydrogen displacements. S^{OO} is also directly related to the DSF (see SM [14]), which is measurable by IXS. The unit vector $\hat{\mathbf{n}}$ in Eq. (2) has been introduced to study the longitudinal or transverse vibrational character. As for the IXS spectra, the thermal average $\langle S^{\mathrm{OO}}_{\hat{\mathbf{n}}}(\mathbf{Q},\omega)\rangle$ has been calculated. Results are shown as color-coded intensity maps in Fig. 3.

If we were studying the vibrations of an actual bcc oxygen crystal (decoupled from hydrogen), the intensity maps of Figs. 3(a) and 3(b) would appear as single well-defined bright lines. Instead, Fig. 3 displays bands broadened by the configurational disorder. It is however clear that vibrations of ice VII still display the main features of the acoustic branches of a simple monoatomic bcc crystal. Indeed, as a guide to the eye, Figs. 3(a) and 3(b) also show the phonon dispersion obtained from a simple four-parameter (up to the second-nearest neighbors) Born-von Kármán model [30] (see SM [14] for details), which reproduces well the main trends of the intensity maps. The acoustic vibrations in disordered ice VII therefore clearly inherit the periodicity of the underlying oxygen bcc sublattice. This is true to such an extent that the distinction between transverse and longitudinal branches remains partially valid even if the cubic point symmetry of the average crystal ($m\bar{3}m$) is lost in most of the individual configurations used for the simulation.

The most important discrepancies between the simple monoatomic bcc picture and the DFT intensity maps are associated to a number of gaps visible on different branches, for example those on both sides of the P point along the [111] direction for the longitudinal branches or that along the [100] direction for the transverse ones. Contrary to other smaller features, these gaps should not be considered as an artifact due to the limited number of configurations employed here. Their presence is due to the fact that ice VII is built from two interpenetrating, but unconnected, hydrogen-bond networks of ice I_c, in each of which the oxygen atoms form a diamond lattice [31]. Direct inspection of the DFT numerical results reveals an important difference between the interatomic force constants of nearest-neighbor oxygen atoms belonging to the same H-bond network or to distinct networks. This asymmetry can be introduced by adding only one parameter to the single atom bcc model, but the crystal then becomes a face-centered cubic with four atoms per cell. The phonon branches of this second model are unfolded in the Brillouin zone of the bcc crystal and are shown in Figs. 3(c) and 3(d) where the size of the dots is directly proportional to the unfolding weight (see SM [14] for details). This modification of the simple bcc model is sufficient to reproduce all the major gap openings observed in the DFT intensity maps. These gaps in the phonon spectrum of ice VII are thus due to its intrinsic structure and should be experimentally detectable.

To further explore these subtle aspects of the ice VII phonon dispersion, unpublished experiments performed on a single crystal [11] have been reinvestigated. An ice VII single crystal was obtained by a slow growth of a single germ from the melt at 2.6 GPa in a diamond anvil cell under resistive heating. A large crystal was obtained, 300 μm in diameter and 150 μm thick. The single-crystal synchrotron IXS configuration was very similar to that used previously for Argon [32]. ID28 was used in the Si (9,9,9) configuration, which provides an overall energy resolution of 3 meV (at 17794 eV). The scattered photons were energy analyzed by a Rowland circle five-crystal spectrometer.

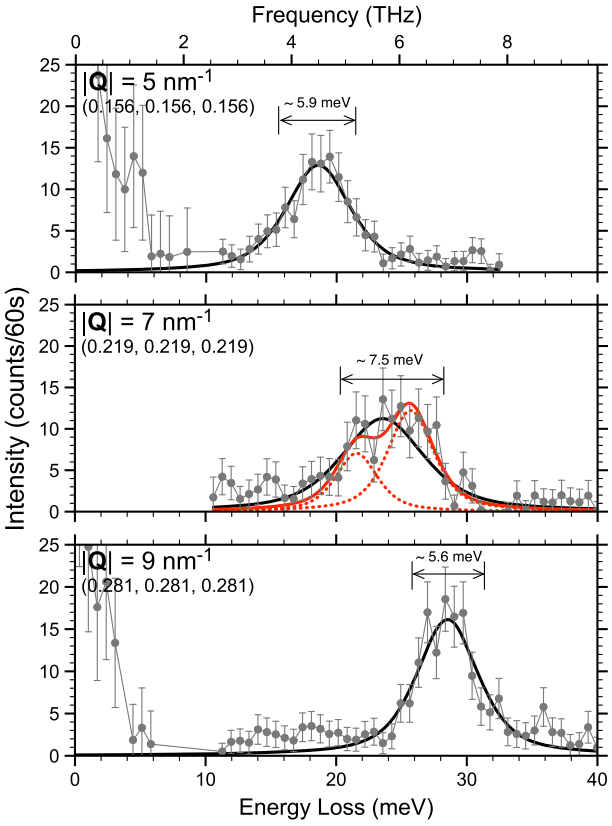

FIG. 4. IXS spectra recorded at 300 K on a single crystal of ice VII at 2.6 GPa along the [111] direction, in the region of the predicted gap. $\mathbf{Q}$-point coordinates are given in $2\pi/a$ unit where a is the lattice parameter of the unit cell. Black lines are used to represent the fits performed with a single pseudo-Voigt. In the case of $|\mathbf{Q}| = 7$ nm^{-1}, an additional fit with two pseudo-Voigt functions is shown in red to mimic the presence of a gap.

A least-squares fit of the longitudinal phonon band along [111] was first carried out using a single pseudo-Voigt function, as shown in black in Fig. 4 (see also SM [14]). The resulting energy position and full width at half maximum (FWHM) are superimposed to the first-principles calculations displayed in Fig. 3(a). An excellent overall agreement is found with the theory although the experimental frequencies are slightly higher than the theoretical ones. Similar trends are also observed on the calculated sound velocities when compared to the measurements performed using Brillouin scattering [33] under high pressure (see SM [14]). These results are indeed not strictly comparable as the single-crystal experiments were collected at 2.6 GPa whereas no such constraint has been imposed during structural relaxation in this Letter. One can, however, notice that the spectra acquired for momentum transfers located at the immediate vicinity of the predicted gaps display a substantially larger linewidth than the neighboring ones. This is visible in the experimental data displayed in Fig. 4, where the FWHM of the spectrum recorded for $|\mathbf{Q}| = 7$ nm^{-1} is ~30% larger than for $|\mathbf{Q}| = 5$ and 9 nm^{-1} and shows an unusual lineshape. Similar results (see SM [14]) are obtained for $|\mathbf{Q}| = 26$ nm^{-1}, i.e. close to the second gap located between H and P. An alternative fit has thus been attempted using two pseudo-Voigt functions for the spectra located in the gap region (see, for instance, the middle panel of Fig. 4), leading to smaller individual linewidths and to a gap of the order of 4 to 6 meV, compatible with the theoretical prediction, as shown in Fig. 3(c). Therefore, despite the limiting signal-to-noise ratio and experimental energy resolution, these results clearly give support to our theoretical predictions.

In summary, our comparison of phonon dispersion in ice VII and its fully proton-ordered counterpart, ice VIII, sheds light on the effect of disorder on the lattice dynamics of these systems. Our main finding is that, despite a full proton disorder in ice VII and the resulting loss of symmetry, acoustic phonon branches inherit the periodicity of the oxygen sublattice, showing the characteristic dispersion of a bcc crystal as well as a largely preserved longitudinal or transverse polarization. While these predictions are clearly confirmed by single-crystal phonon dispersion measurements, our calculations further show that the signature of the specific underlying structure of ice VII, built from two interpenetrating but unconnected hydrogen-bond networks, should appear under the form of well-defined gaps in both longitudinal and transverse acoustic phonon branches. The presence of gaps of the order of 4 to 6 meV is supported by our single crystal data, which show an anomalous phonon linewidth broadening in the corresponding region of the reciprocal space.

We acknowledge access granted to the HPC resources of IDRIS under the allocations A0100910820 and AD010910820R1 made by GENCI (Grand Equipement National de Calcul Intensif). We are grateful to Thierry Strässle (Paul Scherrer Institut, Switzerland) for assisting in the IXS measurements and to P. Giura (IMPMC) for discussions on experimental details.

*Corresponding author: guillaume.radtke@sorbonne-universite.fr
†Corresponding author: stefan.klotz@sorbonne-universite.fr

[1] V. F. Petrenko and R. W. Whitworth, *Physics of Ice* (Oxford University Press, Oxford, 1999).
[2] T. C. Hansen, Nat. Commun. **12**, 3161 (2012).
[3] O. Tschauner, S. Huang, E. Greenberg, V. Prakapenka, C. Ma, G. R. Rossman, A. H. Shen, D. Zhang, M. Newville, and K. Tait, Science **359**, 1136 (2018).
[4] B. Renker, Phys. Lett. **30A**, 493 (1969).
[5] B. Renker, *Lattice Dynamics of Hexagonal Ice*, *Physics and Chemistry of Ice*, edited by E. Whalley, S. J. Jones, and L. W. Gold (Royal Society of Canada, Ottawa; Academic, New York, 1973).
[6] J.-C. Li, J. Chem. Phys. **105**, 6733 (1996).
[7] J.-C. Li and M. Adams, Europhys. Lett. **34**, 675 (1996).
[8] P. T. T. Wong and E. Whalley, J. Chem. Phys. **64**, 2359 (1976).
[9] K. R. Hirsch and W. B. Holzapfel, J. Phys. Chem. **84**, 2771 (1986).
[10] Ph. Pruzan, J. C. Chervin, E. Wolanin, B. Canny, M. Gauthier, and M. Hanfland, J. Raman Spectrosc. **34**, 591 (2003).
[11] P. Loubeyre, R. LeToullec, M. Krisch, and F. Sette, Experimental Report HS-995, European Synchrotron Radiation Facility ESRF, Grenoble, France, 1999.
[12] J. M. Besson, Ph. Pruzan, S. Klotz, G. Hamel, B. Silvi, R. J. Nelmes, J. S. Loveday, R. M. Wilson, and S. Hull, Phys. Rev. B **49**, 12540 (1994).
[13] S. Klotz, J. M. Besson, G. Hamel, R. J. Nelmes, J. S. Loveday, and W. G. Marshall, Nature (London) **398**, 681 (1999).
[14] See Supplemental Material at http://link.aps.org/supplemental/10.1103/PhysRevLett.132.056102 for additional inelastic x-ray scattering data on powder samples of ice VII and VIII and single-crystal measurements on ice VII, details on the density functional theory calculation of the oxygen sublattice dynamic structure factor and on the Born-von Kármán models developed for ice VII.
[15] S. Klotz, Th. Strässle, C. G. Salzmann, J. Philippe, and S. F. Parker, Europhys. Lett. **72**, 576 (2005).
[16] P. Giannozzi *et al.*, J. Phys. Condens. Matter **29**, 465901 (2017).
[17] M. Schlipf and F. Gygi, Comput. Phys. Commun. **196**, 36 (2015).
[18] J. P. Perdew, K. Burke, and M. Ernzerhof, Phys. Rev. Lett. **77**, 3865 (1996).
[19] K. Umemoto, Rev. Mineral. Geochem. **71**, 315 (2010).
[20] K. Komatsu, F. Noritake, S. Machida, A. Sano-Furukawa, T. Hattori, R. Yamane, and H. Kagi, Sci. Rep. **6**, 28920 (2016).
[21] K. Umemoto, R. M. Wentzcovitch, S. de Gironcoli, and S. Baroni, Chem. Phys. Lett. **499**, 236 (2010).
[22] S. Baroni, S. de Gironcoli, A. Dal Corso, and P. Giannozzi, Rev. Mod. Phys. **73**, 515 (2001).
[23] K. Sturm, Z. Naturforsch. **48a**, 233 (1993).

[24] A. Q. R. Baron, in *Synchrotron Light Sources & Free Electron Lasers*, edited by E. J. Jaeschke, S. Khan, J. R. Schneider, and J. B. Hastings (Springer, Berlin, Heidelberg, 2016), Vol. 2, p. 1757.
[25] J.-L. Kuo, J. V. Coe, S. J. Singer, Y. B. Band, and L. Ojamäe, J. Chem. Phys. **114**, 2527 (2001).
[26] J.-L. Kuo and S. J. Singer, Phys. Rev. E **67**, 016114 (2003).
[27] J.-L. Kuo and M. L. Klein, J. Phys. Chem. B **108**, 19634 (2004).
[28] D. D. Klug, J. S. Tse, Z. Liu, X. Gonze, and R. J. Hemley, Phys. Rev. B **70**, 144113 (2004).
[29] K. Umemoto and R. M. Wentzcovitch, Phys. Rev. B **69**, 180103(R) (2004).
[30] P. Brüesch, *Phonons: Theory and Experiments I, Lattice Dynamics and Models of Interatomic Forces* (Springer-Verlag, Berlin, Heidelberg, New York, 1982).
[31] W. F. Kuhs, J. L. Finney, C. Vettier, and D. V. Bliss, J. Chem. Phys. **81**, 3612 (1984).
[32] F. Occelli, M. Krisch, P. Loubeyre, F. Sette, R. Le Toullec, C. Masciovecchio, and J.-P. Rueff, Phys. Rev. B **63**, 224306 (2001).
[33] H. Shimizu, M. Ohnishi, S. Sasaki, and Y. Ishibashi, Phys. Rev. Lett. **74**, 2820 (1995).